Semiconductor Optoelectronics, *Vol. 41 No. 12 (2022), 1567-1579*
https://bdtgd.cn/

STRUCTURAL, SPECTRAL, OPTICAL, MECHANICAL, THERMAL, AND ANTIBACTERIAL STUDIES OF GUANIDINIUM CARBONATE SINGLE CRYSTAL FROM CYANOACETIC ACID AS SOLVENT

R.Subash Chandra Bose[1], K.Balasubramanian[2], R.Subramaniyan Raja[3]
[1] Research Scholar (Reg. No.17211072131024)
[1, 2] PG & Research Department of Physics, The M.D.T. Hindu College, Tirunelveli 627010, Tamilnadu, India
(Affiliated to Manonmaniam Sundaranar University, Abishekapatti, Tirunelveli 627012, Tamilnadu, India)
[3] Department of Physics, KPR Institute of Engineering and Technology, Coimbatore-641407, Tamilnadu, India.
Corresponding Author Email id: subashchandrabose@mdthinducollege.org

ABSTRACT

Guanidinium carbonate (GC) organic crystals of high purity were produced using the time-taken evaporation methods. Crystal X-ray diffraction (XRD) techniques identify the crystal structure as a Tetragonal system having space group $P4_12_12$. It was determined using Fourier Transform Infrared Analysis that the formed crystal contained the functional groups of interest. Based on our optical testing, we comprehend that the ultraviolet (UV) blocking wavelength is somewhere about 239 nm. Specifically, the crystal's optical band gap has been determined to be 5.34 eV after it had grown. Mechanical attributes of the eponymous chemical are obtained from Vicker's microhardness tester. The Nd: YAG laser er employed for establishing the threshold for surface laser damage of the produced crystals. TGA/DTA studies have been performed to investigate thermal behavior. Antifungal action against E. coli as well as Staphylococcus aureus has been investigated as well using the agar diffusion technique.

Keywords: Organic material, slow evaporation, optical studies, mechanical studies, Laser Damage Threshold, NLO

1. Introduction

Many different types of optical devices, including optical toggle switching systems, optical bistable devices, optical modulators, as well as electro-optical structures, need the usage of nonlinear optical (NLO) constituents. [1]. The material used must be a constructive NLO that may be used in optical device usage. Improved NLO compounds could be designed, device functionality could be enhanced, and new materials might be invented using this knowledge. The inorganic and organic molecules, along with the Π-Π bondings, hydrogen bondings, the transfer of charge, as well as the exchange of electrons that determine their solid framework, make this a difficult process. Organic NLO crystals outperform inorganic alternatives because of their elevated nonlinear coefficients, broadband gaps, and resistance to

laser degradation. [3, 4]. To boost the molecule's nonlinear polarisation, organic materials often have an electron/acceptor group introduced into the structure of the molecule. Guanidinium ion, one of several organic molecules, is a simple action that may form a diverse hydrogen-bonded crystal family [5]. There are six possible locations for donors for hydrogen bonding relationship in guanidinium [6, 7], making it an extremely powerful base material that reacts well with typical organic acids and yields an excellent crystalline result. Guanidinium carbonate single crystal was studied for its spectral, antibacterial, social, optical, thermal energy is, as well as mechanical characteristics in an environment of cyanoacetic acid.

2. Experimental Procedure

2.1. Crystal Growth

We used an equimolar mixture of cyanoacetic acid as well as the easily obtainable salt of guanidinium carbonate (AR Grade). Salts were dissolved using double-distilled water prepared at ambient temperature until the correct concentration has been reached. Saturation was achieved after 6 hours of vigorous stirring with a temperature-regulated magnetic stirrer. Clear crystalline GC salt was obtained by filtering the solution that was saturated through Whatman filter paper then allowing it to evaporate at the ambient temperature. Upon 45 days of recrystallization, excellent clear colorless single crystals of the synthesized salts have been obtained and displayed in Fig (1).

Figure 1. grown Guanidinium Carbonate

3. Characterization

3. Results and Discussion

The Single Crystal XRD results indicate the GC Crystal is of the Tetragonal system as well as their space group is $P4_12_12$. The Unit cell constraintss are a=6.98 Å, b=6.94 Å, c=19.65 Å, and V=957 (Å) ^{3} with $\alpha=\beta=\gamma=90^0$.

3.1. PXRD Analysis

PXRD (Powder XRD) examinations were done on finely ground powder of the manufactured specimens of grown crystals. The values are obtained at room temperature, whereas the wavelength of the source was about 1.54 microns. Both 2-step size (0.0200), as well as the time of scan (80 sec), were set in stone. The excellent crystalline quality of the generated samples has been confirmed by the XRD image, which shows crisp diffraction peaks. [8]. Applying the 2 values, the distance

in degrees between the diffraction peaks was determined. In Fig. (2), we see the grown crystal's indexed PXRD pattern.

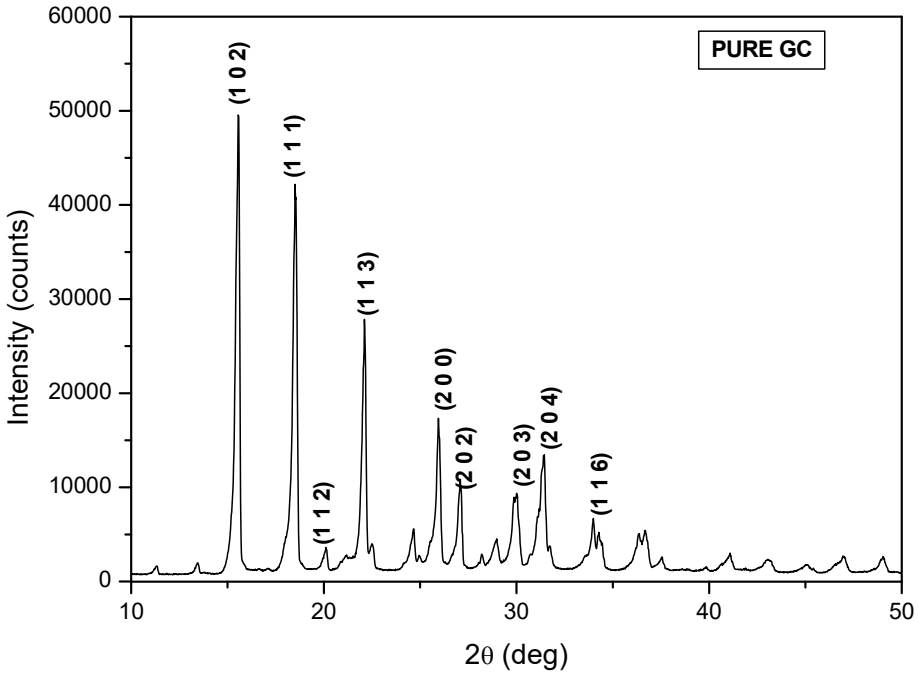

Figure 2. PXRD Graph of Guanidinium Carbonate Single Crystal

3.2. FTIR (Fourier Transform Infrared Analysis)

FTIR analysis results were collected employing the KBr pellet method and a Perkin Elmer FTIR Spectrum RXI Spectrometer. These FTIR spectra, obtained at ambient temperature and shown in Fig. 3, span the wavelength at 400–4000 cm^{-1}. The 3300 cm^{-1} wide band within the spectra is the result of C-H stretches. The N-H asymmetry absorption at 3339 cm^{-1}, as well as 2829 cm^{-1}, causes it to overlap alongside the typical broadband. O-H stretches to account for the observed peaks of 3268 as well as 3197 cm^{-1}. [9] From table1 you can see that GC crystal has all functional groups.

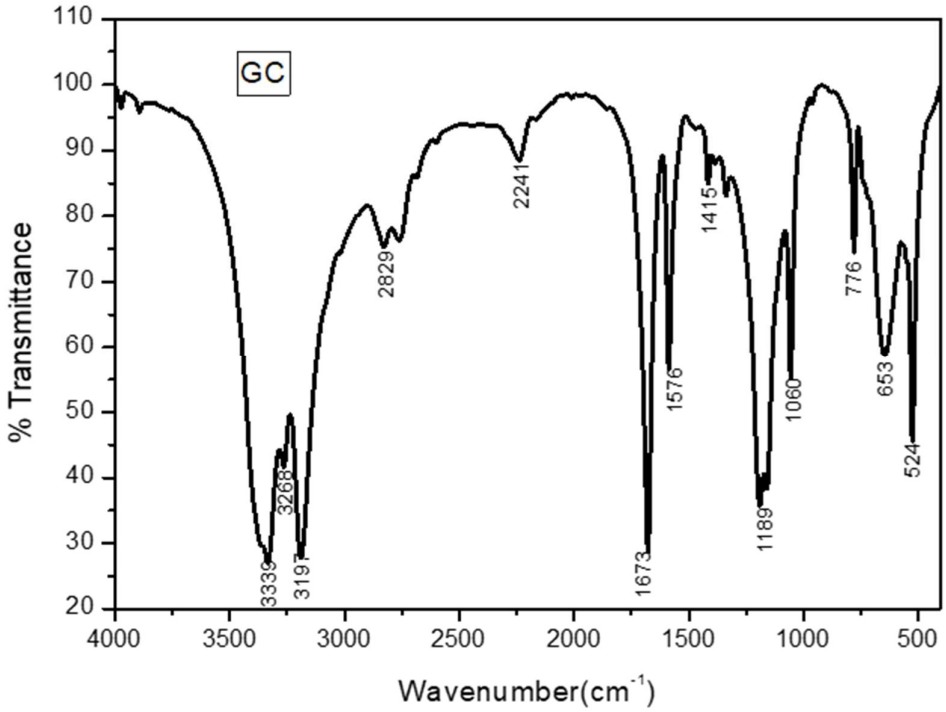

Fig.3. FTIR Spectroscopy of GC

Table 1 Functional group assignments

Wavenumber (cm^{-1})	Stretching	Wavenumber (cm^{-1})	Stretching
3339	N - H	1415	O – H Bending (carboxylic Acid)
3268	O - H (Strong)	1189	C – O
3197	O - H (Weak)	1060	S = O
2829	N - H	776	C – H
2241	C ≡ N	653	C = C
1673	C = N	524	C – Br
1576	C = C		

3.3. Optical Characterization

3.3.1. Optical absorption Analysis

The optical quality of GC crystal is indicative of its suitability and accountability for use in a wide range of devices. The UV-Vis absorption spectrum of GC crystal is depicted in Figure 4. There is unmistakably no indication of electronic transition-related absorption here. The formed crystal has reduced cut-off wavelengths of 239.46 nm as well as shows great transparency across the visible area, both of the characteristics that are indicative of the crystal's functionality for nonlinear optical uses.[10]

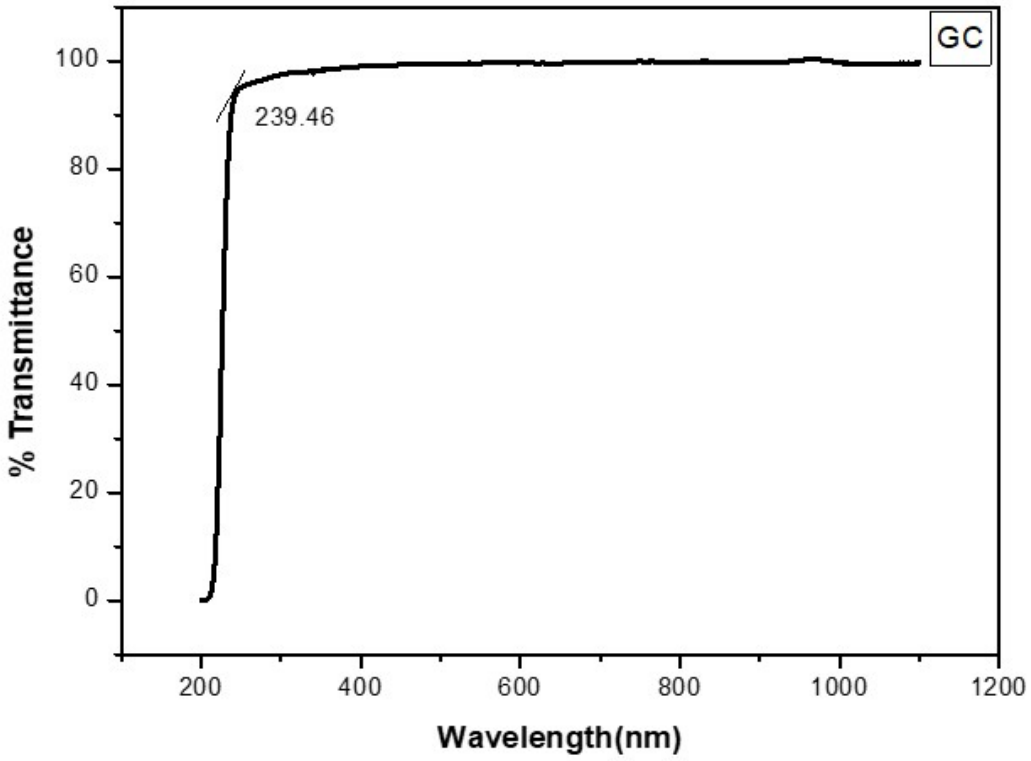

Fig.4. Transmittance Spectra of Grown GC Crystal

3.3.2. Optical Bandgap Calculation

The optical absorption coefficient (α) within a GC crystal being a function of photon energy (E) was determined and measured to learn more about the arrangement of bands and transitions between electrons of the material in question.

$$\alpha = [2.303 \log ((1/T)] / t]$$

Here T indicates crystals Transmittance, t represents the crystal thickness. The figure is plotted with $(\alpha h\upsilon)^2$ with respect to the function of (hυ) Figure 5 depicts this phenomenon, and its linear areas may be extrapolated from there. The generated crystal's optical band gap has been obtained as 5.34 eV. The increased band gap energy of the formed GC crystal is evidence that it is an insulator and has high visible-light transmission. Several optical devices, including optical switches as well as electro-optic modulators, rely on this characteristic of the formed GC crystal. [11]

The absorption coefficient concerning the photon energy is

$$\alpha h\upsilon = \beta (h\upsilon - E_g)^n$$

When E_g represents the optical energy gap as well as n dictates a number that uniquely identifies the optical absorption mechanism and varies in value depending on the type of transition being considered. A direct allowed transition occurs at n=1/2, non-metal substances occur at n=1, a direct forbidden transition occurs at n=3/2, an indirect transition occurs at n=2, and an indirect forbidden transition occurs at n=3. [12] Here, we see that the visual transition is a direct permitted transition since n = 1/2. [13].

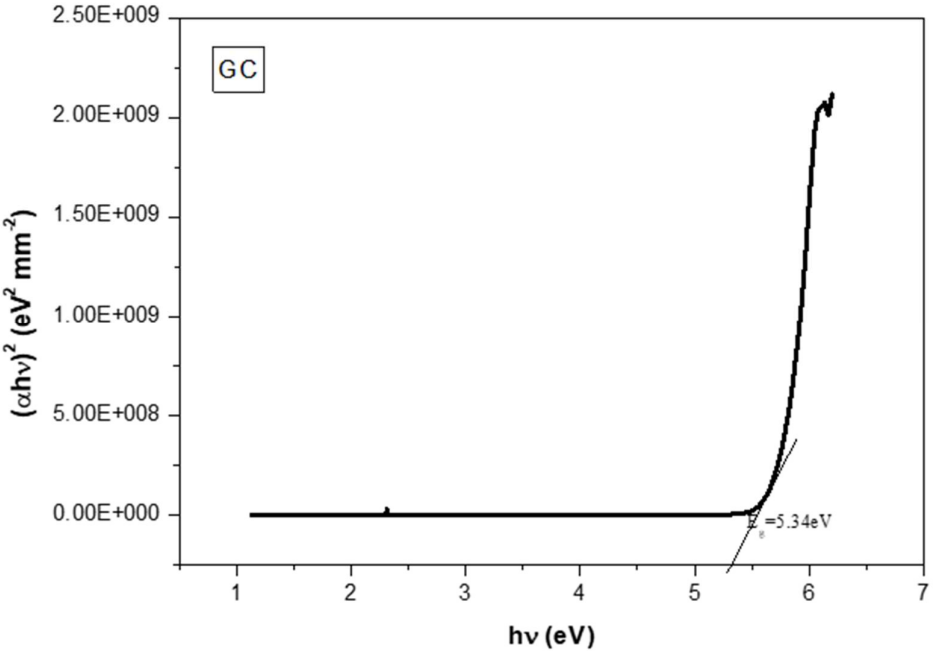

Fig.5. Tauc Plot graph of GC Crystal

3.4. Microhardness Studies

The Vickers microhardness requirement led us to settle on the polished Guanidinium Carbonate Single Crystal. The generated crystal was subjected to a static indentation test with weights ranging from 10 -100 g employing a Vickers diamond pyramid indenter connected with incident ray microscope. After unloading, the indentation mark was calculated with the help of a calibrated micrometer affixed to the microscope's lens, and the average of the diagonal lengths(d) has been plotted fpr every load P.

Using a standard formula, we determined the Vickers microhardness to be

$$H_v = 1.8544\ P / d^2\ (kg/mm^2)$$

Here P indicates applied force in kilos, d depicts diagonal measurement in millimeters. Figure 6 shows how to estimate the inaccuracy in the hardness number Hv. presents a load vs. Hv plot. Crack initiation and material chipping become considerably over 100 g, making it impossible to do the hardness test at that weight. Whenever the indentation load is increased, it is observed that the material's hardness also rises. The size impact of indentation is reversed in the formed crystal [14].

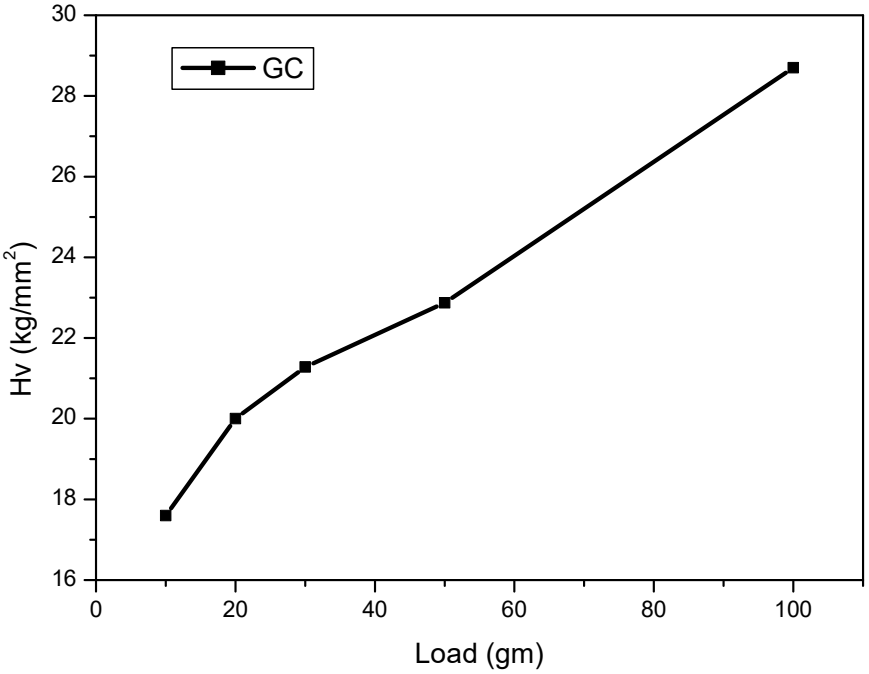

Fig. 6. Load versus Hardness Number of GC Crystal

Meyer's law establishes a correlation between indentation size and applied force, as shown by

$$P=kd^n$$

Slope of the log(P) vs log(d) plotting is depicted as Fig. 7, complete accord using Meyer's law. Analysis of the slope led to the determination that n = 2.5, which is Meyer's index number. If n > 1.6, Ointsch says that the material is hard. Therefore, the GC crystal must be a soft substance, as previously stated. [15]

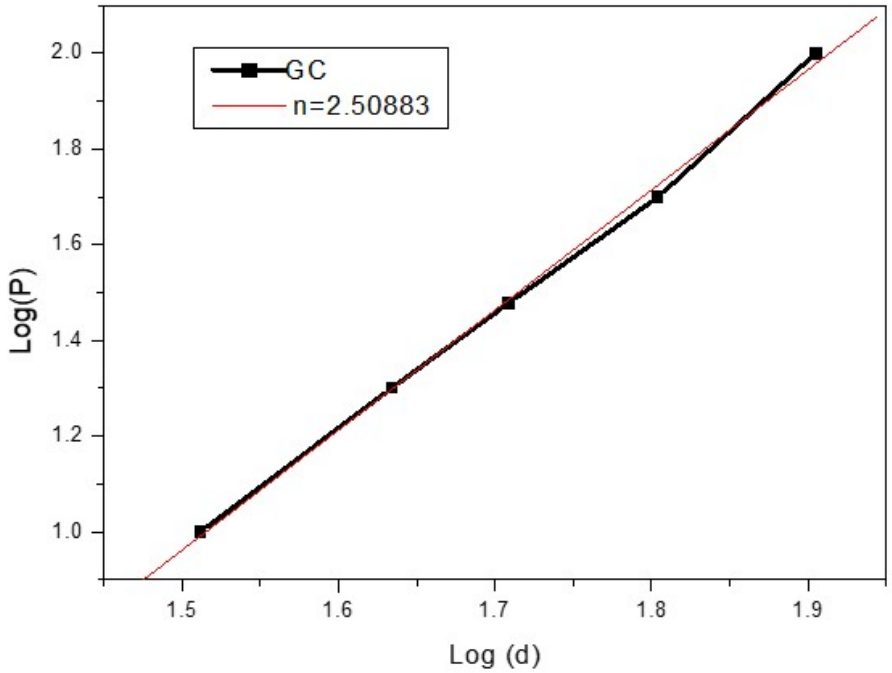

Fig.7. LogdD versus Log P graph of GC Crystal

3.5. Thermal Analysis

GC crystals' thermal properties have been investigated via TG/DTA analysis. This study was conducted on each sample to learn about their thermal expansion and contraction as well as the multiple endothermic and exothermic transitions occurring inside the samples when the temperature has been varied. Crystals are heated with 5ºC/min heating rate in a nitrogen-waft environment contained within a sealed room. Figure 8 displays the TG/DTA curves for GC crystals. The TG curve gives a numerical value for the relative mass change that occurs during the phase change. It demonstrates that the cloth disintegrates and shrinks in volume upon melting. GC crystal revealed two distinct weight loss ranges, as seen in the TG plot. A progressive decrease in mass is depicted by the curve. According to graph, body-weight loss begins at about 139.3 ºC and increases at about 276.4 ºC. DTA analysis shows that the melting point of the sample is 218.4ºC, which occurs simultaneously with the breakdown. Decomposition levels 2 cover the temperature range of 276.4 C - 409.08 ºC. Upon arrival, the residue is 648.8 ºC. The well-known TG investigation indicates that the sample decomposes entirely in the first stage, with just a trace of the potentially harmful gases (carbon, nitrogen, and oxygen) remaining behind [16]. What's more, the crystals break apart devoid of melting or changing shape in any way during the process. The TG/DTA outcome demonstrates an appropriate thermal equilibrium for an NLO crystal.

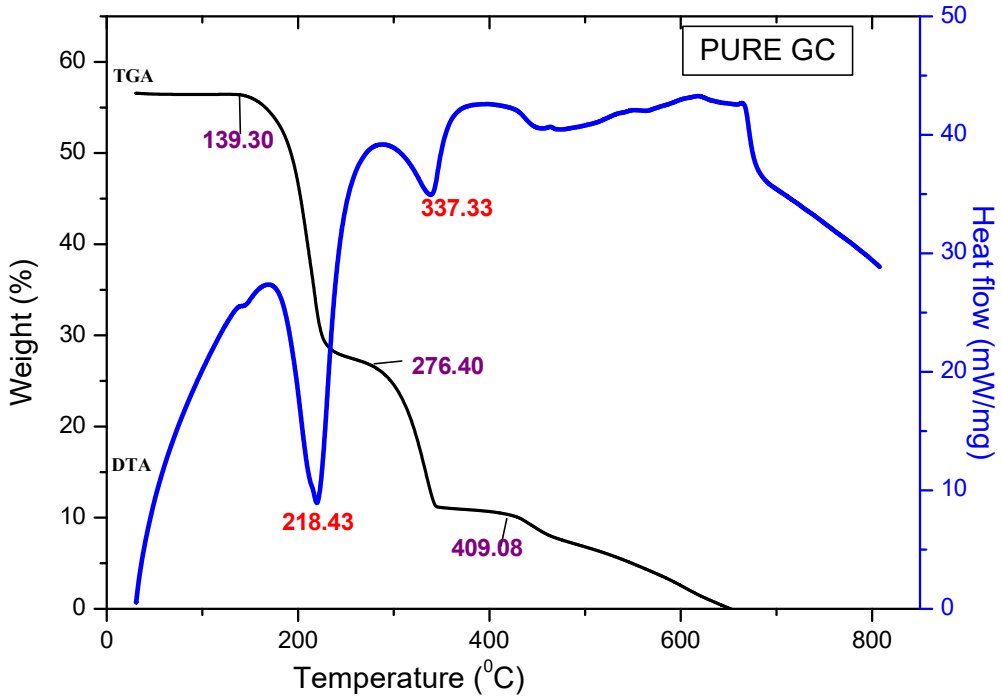

Fig. 8. TG/DTA Curve

3.6. Laser Damage threshold measurements

The LDT has been determined by cutting a block of GC crystals 3mm thick rectangular. For this study, we employed a Q-switched Nd: YAG laser having 1064nm

to take observations. The crystal is placed within the center of a beam having a 45 m diameter and a 10 cm focal length. Various intensities were swept over the GC crystal's surface at a constant pulse rate of 6 ns [17]. At first, a dot appears on the LA crystal's surface having the laser beam's strength (measured in mJ) rise. The GC single crystal then cracks and sustains significant damage as a result. There was breakage at 90mJ.

3.7. NLO Studies

Nonlinear optical (NLO) components are vulnerable to optical damage, which can have serious consequences for high-power laser system functionality [18]. A substantial damage threshold exists, thus, a crucial feature of NLO crystal. Crystals' resistance to laser damage has been determined with the equation

$$\textbf{Power Density (Pd)} = \frac{\mathrm{E}}{\tau\pi r^2}$$

In this equation, E represents energy (mJ), pulse width (ns), as well as r the spot radius (mm). Table 2 compares the harm-caused threshold for several NLO crystals and shows that the laser damage threshold is 9.5GW/cm2. When it comes to the preliminary screening of second harmonic materials production, the Kurtz-Perry powder method is still a helpful instrument. The output power intensity of GC crystal 1.5 times greater than KDP crystal when compared to a KDP sample utilized as a standard.

Table 1

Laser damage thresholds in several NLO-crystals comparison.

Compounds	SHG Efficiency	Laser Damage Threshold (GW/cm^2)
Potassium dihydrogen phosphate (KDP)	1	0.2
Guanidinium Carbonate**	1.5	9.5
Potassium titanyl phosphate (KTP)	1.5	9.5
L-phenylalanine-L-phenylalanine perchlorate	1.4	7.4
L-Asparaginium L-tartarate (AST)	1.5	8.1

** Present work

3.8. Antibacterial Studies

The effectiveness of an antibacterial agent is very sensitive to particle size (between 50 & 750 nm). Biofilms are bacteria that may develop on the outermost layers of retrieved crystalline samples, encouraging further bacterial growth. To verify this, an antibacterial mechanism investigation was conducted on the crystallized GCCA as well as the obtained specimen was tested against two different types of bacteria: E. coli & Staphylococcus aureus. Agar diffusion testing was used to examine the antibacterial properties of the sample. Reference: Van der Watt and colleagues (2001). Inoculating in nutritional broth media and growing at 37% till 18 hours yielded a stock containing bacteria including K.Pnemoneae, Staphylococcus, Bacillus, as well as E. coli. The agar plates for the aforementioned medium were made. Bacterial cultures that had reached 18 hours old had been wiped into sterile plates and used to inoculate each of the plates. The extract should be poured into the five wells at a rate of 1%, 0.1%, 0.01%, and 0.001%. After 24 hours of incubation at 37ºC, the diameter of the inhibitory zone on each plate was measured in centimeters.

Table: Inhibition zone values of E.Coli and S.aureus on various concentrations of GCCA sample

Concentration	*E.Coli (cm)*	*Staphylococcus aureus (cm)*
25 ul	0.8	0.5
50 ul	1.3	1.2
75 ul	1.8	1.7
100 ul	2.0	2.0
STD	2.2	1.8

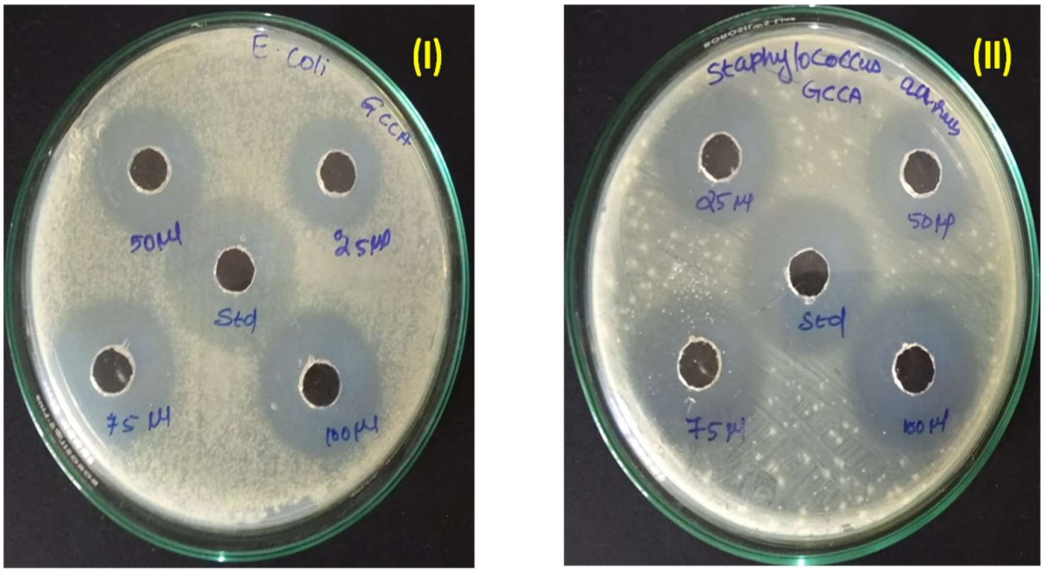

Fig. 9. Antibacterial activity of GCCA Crystals (I) E.coli (II) Staphylococcus Aureus

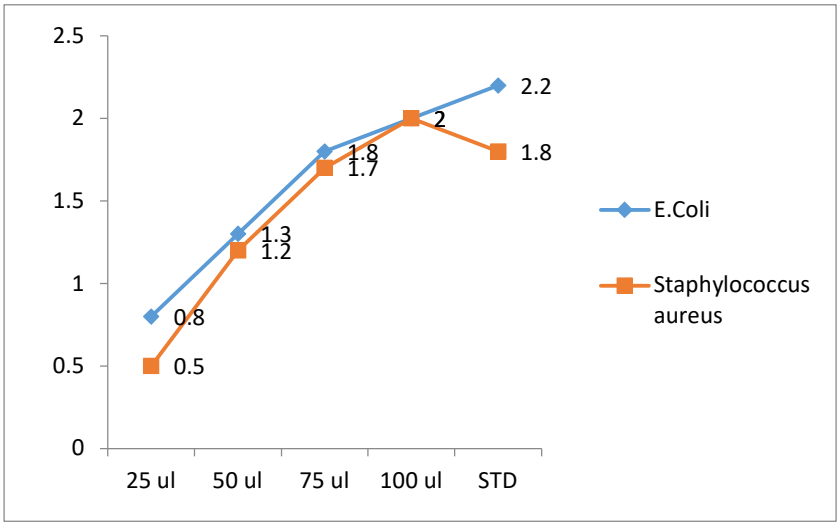

Fig. 10 Inhibition zone variation of (I) E.coli (II) Staphylococcus Aureus

The figure depicts antibacterial mechanism of the grown sample of both gram-negative and gram-positive stains. After incubation around each well, the antibiotic zone scale was used to calculate the absence of bacterial growth around the zone of inhibition. The data suggest that the increased antibacterial activity of the GCCA sample against E.Coli and Staphylococcus aureus bacterial strains may be due to surface-free energy, which determines bacterial adhesion onto crystal surfaces. Susceptible strains have an inhibition zone that is greater for sensitive strains than for resistant ones. [19]. The high antibacterial activity can destroy the bacterial cells found in E.Coli the gram-negative bacteria than S.aures, which may be due to hydrogen bonding interactions that effectively prevent biofilm-related problems in the title GCCA sample which is suitable for biological applications [20].

4. Conclusion

Crystals of guanidinium carbonate were produced upon ambient temperature with the help of a lower evaporation technique using cyanoacetic acid as the solvent. XRD analysis verifies that the formed crystal possesses a tetragonal structure having a space group of $P4_12_12$.Functional groups were detected by FT-IR analysis. Low absorbance at 239.46 nm within UV-Visible spectra of the GC Crystal's curves indicates that its optical bandgap is 5.34 eV, as established by optical absorption tests. Studies of the GC crystal's microhardness have validated the material's softness and hinted at its potential usefulness in device construction. The threshold for LASER damage is 9.5 GW/cm^2. The obtained SHG efficiency was approximately 1.5 times greater than the KDP crystal at that early period. As a result, it was possible to verify that the GC crystals were indeed NLO substances. The antifungal activity of grown GC Crystal can destroy bacterial cells due to hydrogen bonding interactions that effectively prevent biofilm-related problems, GC Crystal is suitable for biological applications like food sciences, medical sciences, and agriculture.

Acknowledgment

The management of The M.D.T Hindu College, Pettai, Tirunelveli, is to be thanked for allowing the authors access to the department's research spaces including the DST-FIST

sponsored instrumentation laboratory.

References

1. P.N.Prasad, D.J.Wollians, Introduction to Nonlinear Optical Effects in Molecules and Polymers, Wiley-Interscience, New York 1991.
2. Nazirahmed, Ahmad.M.M., Kotru.P.N., Single crystal growth by gel technique and characterization of lithium hydrogen tartrate J.Crystal Growth 412 2015: pp.72-79, https://doi.org/10.1016/j.jcrysagro.2014.11.034.
3. T.Baraniraj, P.Philominathan, Growth and Characterization of organic nonlinear optical material:Benzilic acid, J.cryst.Growth 311(2009) 3849-3854.
4. V.Sivashankar, R.Siddheswaran, T.Bharathasarathi, P.Murugakoothan, Growth and Characterization of new semi organic nonlinear optical zinc guanidinium sulfate single crystal, J.Cryst.Gowth 311 (2009) 2709-2713.
5. Beatrice Fraboni, Alessandro Fraleoni-Morgera, Yves Geerts, Albero Morpurgo, Vitaly Podzorov, Organic Single Crystals: An Essential step to New Physics and higher performances of Optoelectronic Devices Adv.Fun,Mater,26(14) 2016. Pp2229-2232. https://doi.org/10.1002/adfm.201504924
6. A.Suvitha, P.Murugakoothan, Synthesis, growth, structural, spectroscopic and optical studies of semiorganic NLO crystal: zinc guanidinium phosphate, Spectrochim, ACta Part A 86(2012) 266-270.
7. https://dx.doi.org/10.1016/j.jjleo.2015.10.159
8. J.M.Adams, R.W.H.Small, The crystal structure of guanidinium carbonate, Acta Crystallogr, B30 (1974)2191.
9. R.K.Khanna, P.J.Miller, Spectrochim. Acta A26 (1970) 1667.
10. T.Arumanayagam, P.Murugakoothan, optical and electrical properties of a new organic nlo crystal: guanidinium 1-monohydragenetartrate 1-tartaric acid Optoelectron. Adv.Mater, 6(12) 2012: pp 263-265.
11. R. E. Denton, R. D. Campbell, S. G. Tomlin, J. Phys. D: Appl. Phys. 1972, 5, 852.
12. S.Ananthi, M.Rajalakshmi, T.S.Shyju, R.gopalakrishnan, Growth and Characterization of an aauct 4-aminobenzoic acid, J.Cryst.Growth 318 (2011)774-779.
13. B.Deepa, P.Philominathan, Optical, Mechanical and thermal behavior of Guanidinium Carbonate single crystal, Optik 127 (2016) 1507-1510
14. D.Sathya, V.Sivashankar, D.Prem Anand, R.Murugesan, Structural, optical, mechanical studies of Guanidine Tartrate single crystal, IJSRSET184166, 2018, pp 393-399
15. B.Deepa, P.Philominathan, Optical, Mechanical and thermal behavior of Guanidinium Carbonate single crystal, Optik 127 (2016) 1507-1510
16. J.Mary Linet, S.Jerome Das, Spectral, Thermal and Hardness Studies on unidirectional grown dichloride diglycine zinc dehydrate single crystal, Physica B 406(2011) 836-840.
17. John Coates, Interpretation of Infrared Spectra, a Practical Approach, Coates Consulting, Newtown, USA.

18. V.V. Azarov, et al. J.Quantum Electron. (1985) 15, 89.
19. Geetha Palani, Arul H, Sengottain Shanmugan & Chithambaram V, *Materials Research Innovations,* **25,** (2020), 331-337.
20. S.Anciya, A.S.I Joy Sinthiya, P. Selvarajan and R.Sree Devi, *Materials Today Proceedings* 49 (2022) 2276-2282.